Mon. Not. R. Astron. Soc. **364,** 433–442 (2005) doi:10.1111/j.1365-2966.2005.09367.x

The radial velocity dispersion profile of the Galactic halo: constraining the density profile of the dark halo of the Milky Way

Giuseppina Battaglia,[1⋆] Amina Helmi,[1] Heather Morrison,[2] Paul Harding,[2] Edward W. Olszewski,[3] Mario Mateo,[4] Kenneth C. Freeman,[5] John Norris[5] and Stephen A. Shectman[6]

[1]*Kapteyn Astronomical Institute, University of Groningen, PO Box 800, 9700 AV Groningen, the Netherlands*
[2]*Astronomy Department, Case Western Reserve University, Cleveland, OH 44106, USA*
[3]*Steward Observatory, University of Arizona, Tucson, AZ 85721, USA*
[4]*Astronomy Department, University of Michigan, Ann Arbor, MI 48109, USA*
[5]*Research School of Astronomy & Astrophysics, The Australian National University, Mount Stromlo Observatory, Cotter Road, Weston ACT 2611, Australia*
[6]*Carnegie Observatories, 813 Santa Barbara Street, Pasadena, CA 91101, USA*

Accepted 2005 June 23. Received 2005 June 5; in original form 2005 January 25

ABSTRACT

We have compiled a new sample of 240 halo objects with accurate distance and radial velocity measurements, including globular clusters, satellite galaxies, field blue horizontal branch (FHB) stars and red giant stars from the Spaghetti survey. The new data lead to a significant increase in the number of known objects for Galactocentric radii beyond 50 kpc, which allows a reliable determination of the radial velocity dispersion profile out to very large distances. The radial velocity dispersion shows an almost constant value of 120 km s^{-1} out to 30 kpc and then continuously declines down to 50 km s^{-1} at about 120 kpc. This fall-off puts important constraints on the density profile and total mass of the dark matter halo of the Milky Way. For a constant velocity anisotropy, the isothermal profile is ruled out, while both a dark halo following a truncated flat (TF) model of mass $1.2^{+1.8}_{-0.5} \times 10^{12}\,\mathrm{M}_{\odot}$ and a Navarro, Frenk & White (NFW) profile of mass $0.8^{+1.2}_{-0.2} \times 10^{12}\,\mathrm{M}_{\odot}$ and $c = 18$ are consistent with the data. The significant increase in the number of tracers combined with the large extent of the region probed by these has allowed a more precise determination of the Milky Way mass in comparison to previous works. We also show how different assumptions for the velocity anisotropy affect the performance of the mass models.

Key words: Galaxy: halo – Galaxy: kinematics and dynamics – Galaxy: structure – dark matter.

1 INTRODUCTION

The determination of the total mass of the Galaxy has been a subject of considerable interest since the work of Kapteyn in the early 1920s (see Fich & Tremaine 1991 for an introductory review on the subject). Since then, the mass of the Milky Way has seen its estimates grow by factors of 10 to 100, with some dependence on the type of mass tracer used: H I kinematics, satellite galaxies and globular clusters, or the Local Group infall pattern. The most recent determinations yield fairly consistent values for the mass within 50 kpc, with an uncertainty of the order of 20 per cent, for a given mass model (Kochanek 1996; Wilkinson & Evans 1999, hereafter W&E99; Sakamoto, Chiba & Beers 2003, hereafter SCB03). However, even today, the total mass of the Galaxy is not known better than within a factor of 2.

Whatever method is used, be it the H I kinematics, globular clusters, satellite galaxies, or halo giants, it is only possible to determine the mass enclosed in the region probed by these tracers (Binney & Tremaine 1987). This implies that the rotation curve derived from H I will only constrain the mass within roughly 18 kpc from the Galactic Centre (Rohlfs & Kreitschmann 1988; Honma & Sofue 1997), a region which is baryon dominated. Globular clusters and satellite galaxies are, in principle, better probes of the large-scale mass distribution of the Galaxy, because they are found out to distances beyond 100 kpc. However, there are only 15 such objects beyond 50 kpc (Zaritsky et al. 1989; Kochanek 1996). Only six of these have proper motion measurements, which, despite the large errors,

⋆E-mail: gbattagl@astro.rug.nl

can further constrain the shape of the velocity ellipsoid. Using this data set, W&E99 favour isotropic to slightly tangentially anisotropic models, although 1σ contours for the velocity anisotropy β give $-0.4 \lesssim \beta \lesssim 0.7$. SCB03 have added to the sample used by W&E99 field blue horizontal branch (FHB) stars with proper motions and radial velocities. While this is clearly an improvement, these stars are located within 10 kpc of the Sun, which strongly limits their constraining power at larger radii. In their models, the velocity ellipsoid is tangentially anisotropic, with $\beta \sim -1.25$ as the most likely value.

It is clearly important to measure the total mass of the Galaxy in order to constrain its dark matter content. However, it is also critical to determine its distribution: density profile, flattening, velocity ellipsoid, etc. One of the most fundamental predictions of cold dark matter (CDM) models is that the density should follow a Navarro, Frenk & White (NFW) profile throughout most of the halo (Navarro, Frenk & White 1997).

The density profiles derived from the gas rotation curves of large samples of external galaxies do not always follow the NFW shape (de Blok, McGaugh & Rubin 2001). Tracers at larger distances are rare, but objects such as planetary nebulae or globular clusters could yield powerful constraints on the mass distribution at those radii; for example, for elliptical galaxies as shown by Romanowsky et al. (2003).

In the case of the Milky Way, the situation is not dissimilar. The distribution of mass inside the Solar circle has been studied extensively (see e.g. Dehnen & Binney 1998; Evans & Binney 2001; Bissantz, Debattista & Gerhard 2004). A common conclusion is that there is little room for dark matter in this region of the Galaxy.

However, does the dark matter beyond the edge of the Galactic disc follow an NFW profile? How does the most often assumed isothermal profile perform in this region of the Galaxy (e.g. Sommer-Larsen et al. 1997; Bellazzini 2004)? Is the velocity ellipsoid close to isotropic as found in CDM simulations (Ghigna et al. 1998)? Modelling of the kinematics of halo stars by Sommer-Larsen et al. (1997) favoured an ellipsoid that became more tangentially anisotropic towards larger distances, while Ratnatunga & Freeman (1989) found a constant line-of-sight velocity dispersion out to 25 kpc.

These fundamental issues can only be addressed when a sufficiently large number of probes of the outer halo of the Galaxy are available. Ideal tracers are red giant stars or blue horizontal branch stars, which can be identified photometrically also at large galactocentric distances (Morrison et al. 2000; Clewley et al. 2002; Sirko et al. 2004a,b). Spectroscopic follow-up allows both the confirmation of the luminosity class as well as the determination of radial velocities with relatively small errors (Morrison et al. 2003). With the advent of wide field surveys, such as the Sloan Digital Sky Survey, or the Spaghetti survey, the numbers of such outer halo probes have increased by large amounts, making this an ideal time to address the mass distribution of our Galaxy in greater detail.

This paper is organized as follows. In Section 2.1, we describe the observational data sets used to determine the radial velocity dispersion curve. In Section 2.2, we introduce several mass models for the dark halo of our Galaxy and derive how the line-of-sight velocity dispersion depends on the model parameters. In Section 2.3, we compare the data to the models and derive the best-fitting values of the parameters using χ^2 fitting. Finally, we discuss our results and future prospects in Section 3.

2 THE RADIAL VELOCITY DISPERSION CURVE

2.1 The observational data sets

Our goal is to derive the radial velocity dispersion profile of the Milky Way stellar halo in the regime where it is dominated by the gravitational potential of its dark matter halo. Hence, we restrict ourselves to tracers located at Galactocentric distances greater than 10 kpc, where the contribution of the disc is less important.

We use a sample of nine satellite galaxies, 44 globular clusters, 57 halo giants and 130 FHB stars. The various data sources of this sample are listed in Table 1. It is worth noting that there are 24 objects located beyond 50 kpc in our sample and that we have enough statistics to measure radial velocity dispersion out to 120 kpc as shown in the top panel of Fig. 1. This covers a significantly larger radial range than many previous works, including e.g. Sommer-Larsen et al. (1997), whose outermost point is at 50 kpc.

The red halo giants are from the Spaghetti survey (Morrison et al. 2000). This is a pencil beam survey that has so far covered 20 deg^2

Table 1. Characteristics of the data used in this paper. In all cases, position in the sky, heliocentric distance and line-of-sight velocities are available.

Objects	Number of objects	Source
Globular clusters	44	Harris (1996)
FHB stars	130	Wilhelm et al. (1999), Clewley et al. (2004)
Red halo giants	57	Spaghetti survey
Satellite galaxies	9	Mateo (1998)

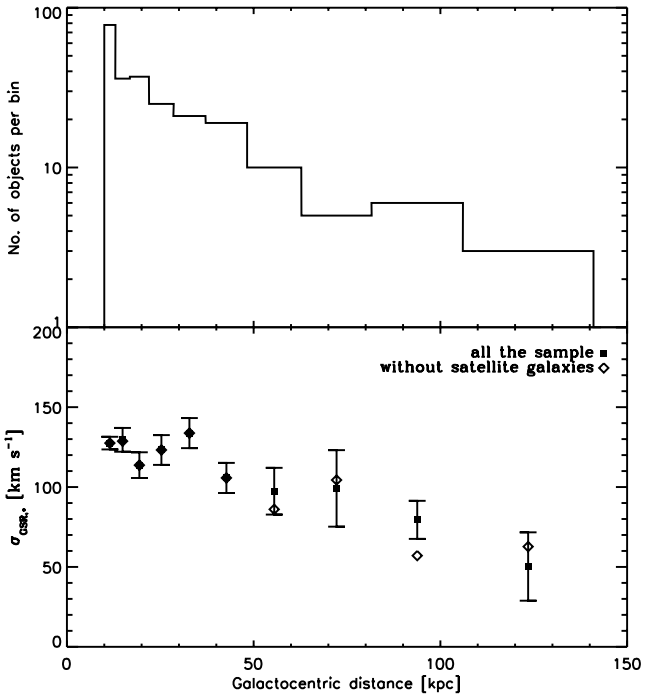

Figure 1. The top panel shows the number of objects per bin in our sample. The bottom panel shows the Galactocentric radial velocity dispersion of the Milky Way halo. The squares with error bars correspond to the dispersion profile for the whole sample. The diamonds indicate the Galactocentric radial velocity dispersion if the satellite galaxies are not included in the sample.

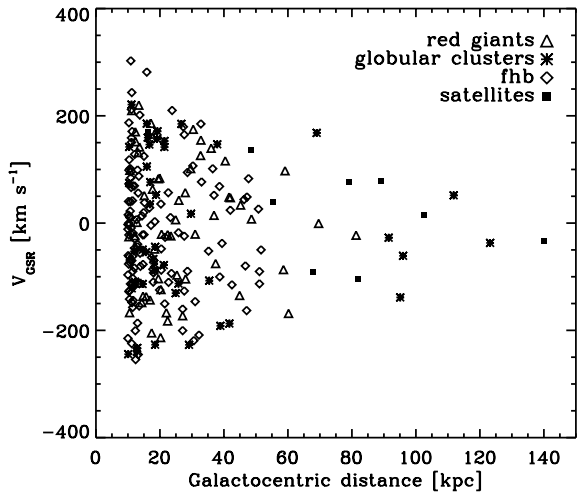

Figure 2. Heliocentric line-of-sight velocities corrected for the Solar motion and the LSR motion ($V_{\rm GSR}$) for the sample used in this work (triangles, red giants; asterisks, globular clusters; diamonds, field horizontal branch stars; filled squares, satellite galaxies).

in the sky, down to $V \sim 20$. It identifies candidate halo giants using Washington photometry, where the 51 filter[1] allows for a first luminosity selection. Spectroscopic observations are then carried out to confirm the photometric identification and to determine the radial velocities of the stars.

We have derived the heliocentric distance for the FHB stars from Wilhelm et al. (1999) using the relation

$$M_V(\mathrm{HB}) = 0.63 + 0.18([\mathrm{Fe/H}] + 1.5)$$

(Carretta et al. 2000).

In all cases, accurate distances and radial velocities are available: the average error in velocity ranges from a few km s^{-1} (satellite galaxies and globular clusters) to 10–15 km s^{-1} (FHB stars and red giants); the typical relative distance error is approximately 10 per cent.

When transforming the heliocentric line-of-sight velocities, $V_{\rm los}$, into Galactocentric ones, $V_{\rm GSR}$, we assume a circular velocity of $V_{\rm LSR} = 220\,\mathrm{km\,s^{-1}}$ at the solar radius ($\mathrm{R}_\odot = 8$ kpc) and a solar motion of $(U, V, W) = (10, 5.25, 7.17)\,\mathrm{km\,s^{-1}}$, where U is radially inward, V positive in the direction of the Galactic rotation and W towards the North Galactic Pole (Dehnen & Binney 1998). Hereafter, we refer to: the radial velocity (dispersion) measured in a heliocentric coordinate system as the line-of-sight velocity, $V_{\rm los}$ (dispersion, $\sigma_{\rm los}$); the line-of-sight velocity (and its dispersion) corrected for the solar motion and the LSR motion as the Galactocentric radial velocity, $V_{\rm GSR}$ (dispersion, $\sigma_{\rm GSR}$); the radial velocity (and its dispersion) in a reference frame centred on the Galactic Centre as the true radial velocity, $V_{\rm r}$ (dispersion, $\sigma_{\rm r}$). Fig. 2 shows $V_{\rm GSR}$ as function of the Galactocentric distance r for all the objects used in this work.

The bottom panel in Fig. 1 shows the Galactocentric radial velocity dispersion as function of distance from the Galactic Centre. This is computed in bins whose width is approximately twice the average distance error of objects in the bin. This implies that our bin sizes range from 3 kpc at $r \sim 10$ kpc to 40 kpc at $r \sim 120$ kpc. The error bar on the velocity dispersion in each bin is calculated performing Monte Carlo simulations. We assume the velocity and distance errors are gaussianly distributed in the heliocentric reference frame. In practice, this means that we randomly generate velocities and distances for each one of the stars, whose mean and dispersion are given by the observed value and its estimated error, respectively. We then convert the heliocentric quantities into Galactocentric ones. We repeat this exercise for 10 000 sets and, for each of these, we measure $\sigma_{\rm GSR}$ in the same bins as the original data. We use the rms of this velocity dispersion, obtained from the 10 000 simulations, as the error on the velocity dispersion we measured in the bin.

One may question whether the satellite galaxies can be considered fair tracers of the gravitational potential of the dark matter halo of the Milky Way (e.g. Gao et al. 2004; Taylor et al. 2004). To get a handle on this issue, we compute the velocity dispersion profile both with and without them (squares and diamonds, respectively, in Fig. 1). Because the trend is similar in both cases, we may consider the satellites to be reliable probes of the outer halo potential.

2.2 The models

2.2.1 Jeans equations

If we assume that the Galactic halo is stationary and spherically symmetric, we can derive the (expected) radial velocity dispersion profile $\sigma_{r,*}$ of the stars from the Jeans equation (Binney & Tremaine 1987):

$$\frac{1}{\rho_*}\frac{\mathrm{d}\left(\rho_*\sigma_{r,*}^2\right)}{\mathrm{d}r} + \frac{2\beta\sigma_{r,*}^2}{r} = -\frac{\mathrm{d}\phi}{\mathrm{d}r} = -\frac{V_{\rm c}^2}{r}, \qquad (1)$$

where $\rho_*(r)$ is the mass density of the stellar halo, $\phi(r)$ and $V_{\rm c}(r)$ are the potential and circular velocity of the dark matter halo, and β is the velocity anisotropy parameter, defined as $\beta = 1 - (\sigma_\theta^2/\sigma_{\rm r}^2)$, and assuming $\sigma_\theta^2 = \sigma_\phi^2$. Note that $\beta = 0$ if the velocity ellipsoid is isotropic, $\beta = 1$ if the ellipsoid is completely aligned with the radial direction, while $\beta < 0$ for tangentially anisotropic ellipsoids.

The Jeans equation allows us to determine a unique solution for the mass profile if we know $\sigma_{r,*}^2(r)$, $\rho_*(r)$ and $\beta(r)$, although this solution is not guaranteed to produce a phase-space distribution function that is positive everywhere. However, we are faced with two uncertainties: the velocity anisotropy and the behaviour of the stellar halo density at very large distances. The latter has been determined to vary as a power law $\rho_*(r) \propto r^{-\gamma}$ with $\gamma \sim 3.5$ out to $\sim$50 kpc (Morrison et al. 2000; Yanny et al. 2000) and we shall assume this behaviour can be extrapolated all the way out to our last measured point. More crucial is the unknown variation of the velocity anisotropy with radius, which is difficult to determine because of the lack of tracers with accurate proper motions beyond the Solar neighbourhood. In principle, this implies that large amounts of kinetic energy can be hidden to the observer, an effect known as the mass–velocity anisotropy degeneracy. For the sake of simplicity, and given that the situation is unlikely to change until the advent of new space astrometric missions such as *SIM* and *Gaia* (Perryman et al. 2001), throughout most of this work we shall make the assumption that β is constant, i.e. independent of radius r.

To derive equation (1), we have assumed that the stellar halo can be considered as a tracer population of objects moving in an underlying potential. This is justified by the negligible amount of mass present in this component, compared with, for example, that in the disc and the dark halo.

The (expected) radial velocity dispersion for the tracer population $\sigma_{r,*}$ may be thus derived by integrating equation (1). This leads

[1] The 51 filter is centred on the Mgb/MgH feature near 5170 Å.

to

$$\sigma^2_{r,*}(r) = \frac{1}{\rho_* e^{\int 2\beta \mathrm{d}x}} \int_x^\infty \rho_* V_\mathrm{c}^2 e^{\int 2\beta \mathrm{d}x''} \mathrm{d}x', \qquad x = \ln r. \tag{2}$$

Here, we have used that $r^{2\beta}\rho_*\sigma_{r,*}|_\infty = 0$. Note that the radial velocity dispersion of the tracer population depends on the particular form of the circular velocity of the underlying (gravitationally dominant) mass distribution.

Because proper motions are not available for the whole sample and we only have access to heliocentric velocities, the quantity that we measure is not the true radial velocity dispersion but $\sigma_{\mathrm{GSR},*}$. When comparing this quantity to model predictions, we must take into account a correction factor for the lack of information on the tangential component of the velocity. Following the procedure described in Appendix A, we find that the Galactocentric radial velocity dispersion, $\sigma_{\mathrm{GSR},*}$, is related to the true radial velocity dispersion, $\sigma_{r,*}$ as

$$\sigma_{\mathrm{GSR},*}(r) = \sigma_{r,*}(r)\sqrt{1 + 2\,(1-\beta)H(r)}, \tag{3}$$

where

$$H(r) = \frac{r^2 + \mathrm{R}_\odot^2}{4r^2} - \frac{\left(r^2 - \mathrm{R}_\odot^2\right)^2}{8r^3\,\mathrm{R}_\odot} \ln\frac{r + \mathrm{R}_\odot}{r - \mathrm{R}_\odot}. \tag{4}$$

The above equation for $H(r)$ is valid at Galactocentric distances $r > \mathrm{R}_\odot$. For a purely radial anisotropic ellipsoid ($\beta = 1$), $\sigma_{\mathrm{GSR},*}$ and $\sigma_{r,*}$ coincide. For a tangentially anisotropic stellar halo, the correction factor becomes negligible at distances larger than about 30–40 kpc.

2.2.2 *Specifing dark matter halo models*

We adopt three different models for the spherically symmetric dark matter halo potential:

(i) *Pseudo-isothermal sphere.* This model has been extensively used in the context of extragalactic rotation curve work. The density profile and circular velocity associated to a pseudo-isothermal sphere are:

$$\rho(r) = \rho_0 \frac{r_\mathrm{c}^2}{\left(r_\mathrm{c}^2 + r^2\right)} \tag{5}$$

and

$$V_\mathrm{c}^2(r) = V_\mathrm{c}^2(\infty)\left(1 - \frac{r_\mathrm{c}}{r}\mathrm{arctg}\frac{r}{r_\mathrm{c}}\right), \tag{6}$$

where r_c is the core radius and $\rho_0 = V_\mathrm{c}^2(\infty)/4\pi G r_\mathrm{c}^2$. We set $V_\mathrm{c}(\infty) = 220\,\mathrm{km\,s^{-1}}$ as the asymptotic value of the circular velocity. At large radii, the density behaves as $\rho \propto r^{-2}$ giving a mass that increases linearly with radius.

(ii) *NFW model.* In this case the dark matter density profile is given by

$$\rho(r) = \frac{\delta_c \rho_\mathrm{c}^0}{(r/r_\mathrm{s})(1 + r/r_\mathrm{s})^2}, \tag{7}$$

where r_s is a scale radius, ρ_c^0 the present critical density and δ_c a characteristic overdensity. The latter is defined by $\delta_\mathrm{c} = 100\,c^3 g(c)/3$, where $c = r_\mathrm{v}/r_\mathrm{s}$ is the concentration parameter of the halo and $g(c) = \frac{1}{\ln(1+c) - c/(1+c)}$. The circular velocity associated with this density distribution is

$$V_\mathrm{c}^2(s) = \frac{V_\mathrm{v}^2 g(c)}{s}\left[\ln(1 + cs) - \frac{cs}{1 + cs}\right], \tag{8}$$

where V_v is the circular velocity at the virial radius r_v and $s = r/r_\mathrm{v}$. The concentration c has been found to correlate with the virial mass of the halo (Navarro et al. 1997; Bullock et al. 2001; Wechsler et al. 2002). However, the relation presents a large scatter. For example, for a halo of mass $1.0 \times 10^{12}\,h^{-1}\,\mathrm{M}_\odot$ the predicted concentration ranges between 10 and 20. Hence, we cannot consider the NFW density profile as a one-parameter family; we need to describe it by the concentration c and by the virial mass or the circular velocity at the virial radius. At large radii (for $r \gg r_\mathrm{s}$), the density behaves as $\rho \propto r^{-3}$ and, therefore, the total mass diverges logarithmically. However, we can impose that the particles must be bound at the virial radius, and so when integrating equation (2), we set the upper integration limit to r_v and we use $\mathrm{r}^{2\beta}\rho_*\sigma_{\mathrm{r},*}|_{\mathrm{r_v}} = 0$.

(iii) *Truncated flat model.* This density profile was recently introduced by W&E99 to describe the dark matter halo of Local Group galaxies. It is a mathematically convenient extension of the Jaffe (1983) model. The form of the density profile of the truncated flat model (hereafter TF) is

$$\rho(r) = \frac{M}{4\pi}\frac{a^2}{r^2(r^2 + a^2)^{3/2}}, \tag{9}$$

where a is the scalelength and M the total mass of the system. For $r \gg a$, the density falls off as $\rho \propto r^{-5}$. The circular velocity due to this density distribution is

$$V_\mathrm{c}^2(r) = \frac{V_0^2 a}{(r^2 + a^2)^{1/2}}. \tag{10}$$

We set $V_0 = 220\,\mathrm{km\,s^{-1}}$ (W&E99). The resulting rotation curve is flat in the inner part, with amplitude $V_0 = \sqrt{GM/a}$, and becomes Keplerian for $r \gg a$. Having fixed the amplitude of the circular velocity (V_0), this model is reduced to a one parameter-family characterized by the scalelength a, or the mass M.

2.3 Results

2.3.1 *Models with constant velocity anisotropy*

The methodology we use consists of comparing the measured Galactocentric radial velocity dispersion $\sigma_{\mathrm{GSR},*}$ for each of the distance bins with that predicted for the different models discussed in Section 2.2. For the latter, we explore the space of parameters that define each model and determine the χ^2 as

$$\chi^2 = \sum_{i=1}^{\mathrm{Nbins}} \left[\frac{\sigma_{\mathrm{GSR}_i,*} - \sigma_{\mathrm{GSR},*}(r_i;\beta,\,p)}{\epsilon_\mathrm{r}}\right]^2. \tag{11}$$

Here, the variable p denotes a characteristic parameter of each model (e.g. scalelength or total mass), while ϵ_r is the error in the observed radial velocity dispersion as estimated through the bootstrap sampling technique described before. The best-fitting parameters are defined as those for which χ^2 is minimized.

In the case of the isothermal sphere, the free parameters are the dark matter halo core radius, r_c, and the stellar velocity dispersion anisotropy parameter, β. The left panel of Fig. 3 shows the χ^2 contours for this model. The minimum χ^2 value is $\chi^2_{\mathrm{min}} = 23$ for $r_\mathrm{c} = 1.6$ kpc and $\beta = -0.4$, with 1σ contours encompassing $0.6 \lesssim r_\mathrm{c} \lesssim 2.6$ and $-0.7 \lesssim \beta \lesssim -0.1$. This corresponds to a best-fitting mass $M = 1.3 \times 10^{12}\,\mathrm{M}_\odot$ (note that, because the mass for the pseudo-isothermal model is not finite, we quote the mass within our last measured point, at $r = 120$ kpc). The 1σ errors on the mass, calculated from the 1σ errors for the core radius, lead to a relative error of the order of 1 per cent. The reason for this small value is due to the fact that the best-fitting core radius is very small and

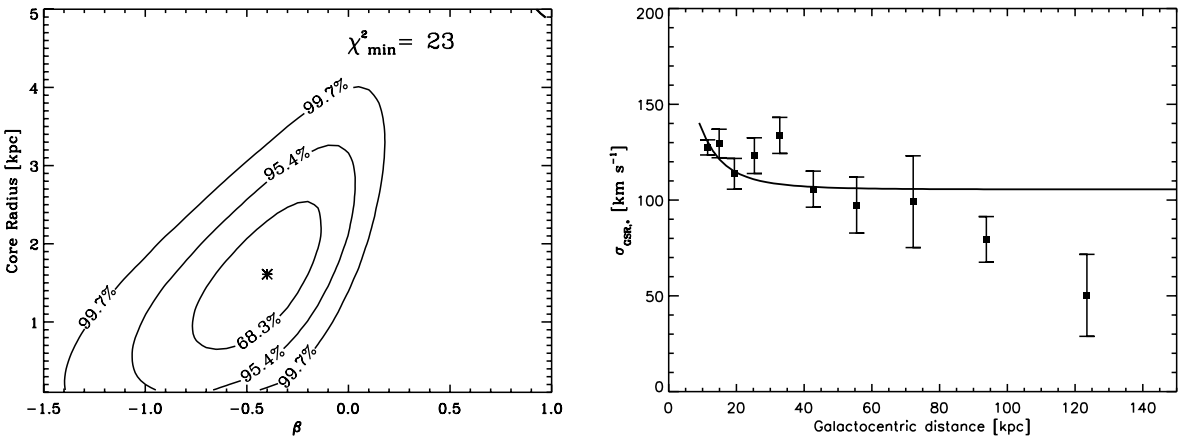

Figure 3. Left: contour plot of $\Delta\chi^2$ corresponding to a probability of 68.3, 95.4, 99.7 per cent (1σ, 2σ, 3σ) for the isothermal sphere model with constant anisotropy. The asterisk indicates the location of the minimum χ^2 (whose value is shown in the upper right corner). Right: observed radial velocity dispersion (squares with error bars) overlaid on the best-fitting model for the isothermal mass distribution (solid line).

hence variations in its value (even by 100 per cent) will barely affect the mass enclosed at large radii. On the right panel of Fig. 3, we plot the Galactocentric radial velocity dispersion for this best-fitting model. As expected, this model predicts a velocity dispersion that is roughly constant with radius. However, the observed $\sigma_{\rm GSR,*}$ shows a rather strong decline at large radii, which is not reproduced by the pseudo-isothermal halo model.

The top panels of Fig. 4 show the χ^2 contours for the NFW model for four different concentrations ($c = 10$, 14, 16 and 18). Note that the minimum χ^2 value decreases for increasing concentrations. Because the concentration is defined as $c = r_{\rm v}/r_{\rm s}$, for a fixed mass (or virial radius $r_{\rm v}$) a larger c implies a smaller scale radius. This results in a radial velocity dispersion that starts to decline closer to the centre in comparison to a halo of lower concentration, reproducing better the trend observed in the data. Our χ^2 fitting technique yields for $c = 10$ a best-fitting virial mass of $1.2 \times 10^{12}\,{\rm M}_\odot$ ($\chi^2_{\rm min} = 36$), while for $c = 18$, $M_{\rm v} = 0.8 \times 10^{12}\,{\rm M}_\odot$ ($\chi^2_{\rm min} = 12$). We find that the velocity anisotropy for the minimum χ^2 is almost purely radial in all cases. In the bottom panel of Fig. 4, we show the observed Galactocentric radial velocity dispersion overlaid on two of the best-fitting NFW models. Note that beyond 40 kpc, the model with $c = 10$ is clearly inconsistent with the data at the 1σ level at $r \sim 40$ and 50 kpc and at the 2σ level in the last two bins. On the other hand, the $c = 18$ model gives a good fit of the data out to 30 kpc but overpredicts the velocity dispersion at large radii at the 1σ level. We thus consider the NFW model with $M_{\rm v} = 0.8^{+1.2}_{-0.2} \times 10^{12}\,{\rm M}_\odot$ and $c = 18$ as producing the best fit. Fig. 4 also shows the favourite model of Klypin, Zhao & Somerville (2002) with $M_{\rm v} = 1.0 \times 10^{12}\,{\rm M}_\odot$ and $c = 12$ (dotted curve). Because no velocity anisotropy was given in the source, we performed a χ^2 fit to our data using the parameters from Klypin et al. (2002) and leaving β as a free parameter. This favoured once again an almost purely radial anisotropy. The fit obtained in this case is very similar to that found in our $c = 10$ model.

Because our last measured point is at $r_{\rm last} \sim 120$ kpc, the constraining power of our data is stronger in the region enclosed by this radius. The value of the virial mass we just derived is an extrapolation of the model at larger distances. For completeness, we quote here the mass within 120 kpc for our best-fitting NFW model with $c = 18$, $M(<120\,{\rm kpc}) = 5.4^{+2.0}_{-1.4} \times 10^{11}\,{\rm M}_\odot$ (the errors are calculated from the 1σ errors in the best-fitting mass).

The left panel of Fig. 5 shows the contour plot for the TF model. Our best fit has a mass of $1.2^{+1.8}_{-0.5} \times 10^{12}\,{\rm M}_\odot$ and $\beta = -0.50 \pm 0.4$ ($\chi^2_{\rm min} = 25$). The mass enclosed in 120 kpc is $M(<120\,{\rm kpc}) = 9.0^{+6.0}_{-3.0} \times 10^{11}\,{\rm M}_\odot$. Our results are compatible with the work of W&E99: they find a mass of $M = 1.9^{+3.6}_{-1.7} \times 10^{12}\,{\rm M}_\odot$, even though they favour a slightly radially anisotropic velocity ellipsoid. The right panel of Fig. 5 shows the data overlaid onto our best-fitting model (solid line). Visual inspection shows that the large value obtained for the minimum χ^2 is driven by the discrepancy between model and data in the bins at 11.5 and 33 kpc. However, at large radii, our TF model with $M = 1.2 \times 10^{12}\,{\rm M}_\odot$ provides a good representation of the data. Fig. 5 also shows that the favourite W&E99 model (dashed curve), having a larger mass and a more radially anisotropic velocity ellipsoid, overpredicts the Galactocentric radial velocity dispersion. On the other hand, the TF model of SCB03, for which $M = 2.5 \times 10^{12}\,{\rm M}_\odot$ and $\beta = -1.25$, i.e. a heavier halo whose ellipsoid is much more tangentially anisotropic, declines too quickly in the inner part and tends to flatten at large radii (dotted curve), not following the trend shown by the data.

The comparison of the fits produced by the constant anisotropy TF and NFW models shows that the latter reproduces better the trends in the data as a whole, from small to large radii. However, at very large radii, it tends to overpredict the velocity dispersion. In this regime, the TF model provides a much better fit. This can be understood as follows. In the region between 50 and 150 kpc, where $\sigma_{\rm GSR,*}$ shows the decline, the slope of the TF model ranges between -3 and -4 whilst the slope of the NFW density profile is around -2.5. This means that, in models with a constant velocity anisotropy, a steep dark matter density profile at large radii is favoured by the data.

2.3.2 *Toy models for the velocity anisotropy*

We will now briefly relax the assumption that β is constant with radius. We shall explore the following models for $\beta(r)$:

(i) *Model β-rad (radially anisotropic).* Diemand, Moore & Stadel (2004) have found in N-body ΛCDM simulations that the anisotropy of subhalo velocities behaves as

$$\beta(r) \simeq 0.35\frac{r}{r_{\rm v}}, \qquad \text{for } r \leqslant r_{\rm v}. \tag{12}$$

We will use this cosmologically motivated functional form to study the effect of an increasingly radially anisotropic velocity ellipsoid in our modelling of the radial velocity dispersion curve.

(ii) *Model β-tg (tangentially anisotropic).* Proper motion measurements of the Magellanic Clouds and Sculptor, Ursa Minor and

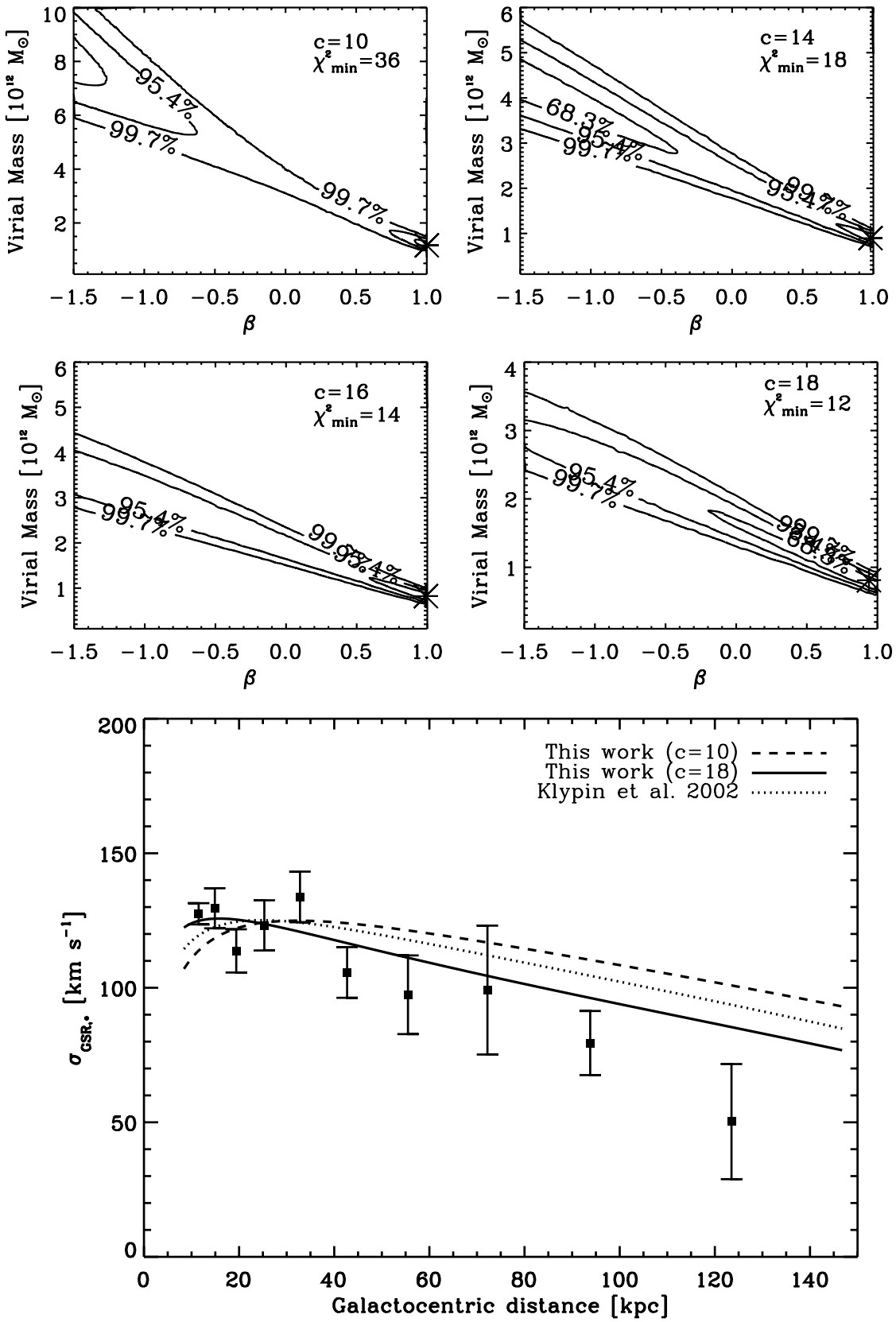

Figure 4. Top: contour plot of $\Delta\chi^2$ corresponding to a probability of 68.3, 95.4, 99.7 per cent ($1\sigma, 2\sigma, 3\sigma$) for the NFW model at four different concentrations. The value of the concentration and minimum χ^2 are shown in the upper right corner of each panel. The asterisk indicates the location of the minimum χ^2 and hence of the best-fitting parameters. The virial mass is given in units of 10^{12} $M_\odot$. Bottom: observed radial velocity dispersion (squares with error bars) overlaid on two of the best-fitting models for the NFW mass distributions (dashed line, $c = 10$; solid line, $c = 18$). The dotted curve corresponds to the Galactocentric radial velocity dispersion profile obtained using the preferred model (B1) of Klypin et al. (2002).

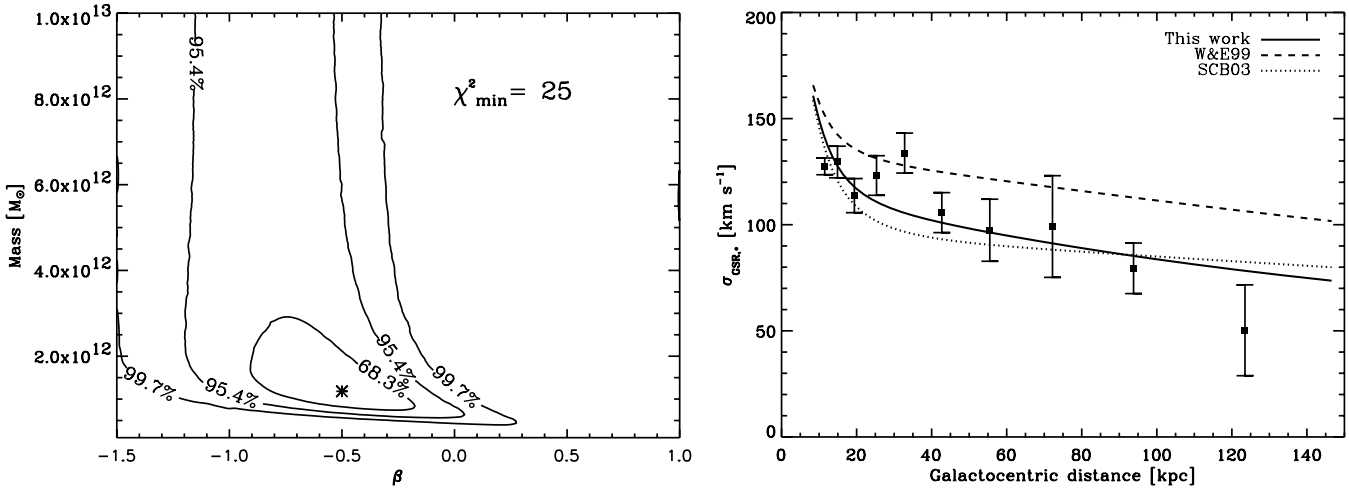

Figure 5. Left: contour plot of $\Delta\chi^2$ corresponding to a probability of 68.3, 95.4, 99.7 per cent (1σ, 2σ, 3σ) for the TF model. The asterisk indicates the location of the minimum χ^2 (whose value is shown in the upper right corner). Right: observed radial velocity dispersion (squares with error bars) overlaid on the best-fitting model for the TF mass distribution (solid line). The dashed line shows the Galactocentric radial velocity dispersion obtained using the best-fitting parameters from previous works (dashed, W&E99; dotted, SCB03).

Fornax dwarf spheroidals suggest that the tangential velocities of these objects are larger than their radial motions (Schweitzer et al. 1995; Kroupa & Bastian 1997; Schweitzer, Cudworth & Majewski 1997; Dinescu et al. 2004). If confirmed, this would have as a consequence that the velocity ellipsoid should be tangentially anisotropic at large radii. To explore the effect on our dynamical models of a velocity ellipsoid that becomes increasingly more tangential, we consider the following toy model:

$$\beta(r) = \beta_0 - \frac{r^2}{h^2}, \tag{13}$$

where we set the scale factor $h = 120$ kpc. We choose two values for β_0: in the first case (model $\beta-\mathrm{tg_{toy}}$); we arbitrarily fix it to 1 in the second model ($\beta-\mathrm{tg_{SN}}$), we use a sample of 91 nearby halo stars from Beers et al. (2000) within 0.5 kpc from the Sun and with [Fe/H] < -1.5 to normalize our model. In this case, we find that $\beta(\mathrm{R}_\odot) = 0.33$ and, therefore, $\beta_0 = 0.33 + \mathrm{R}_\odot^2\, h^{-2}$.

Using the models for $\beta(r)$ described above, we perform again the χ^2 best-fitting procedure for an NFW model of $c = 18$. There is, therefore, in all cases, only one free parameter: the virial mass. The results of this new analysis are shown in the bottom panel of Fig. 6. The $\beta-$rad model, for which the velocity ellipsoid becomes more radially anisotropic with radius, has $\chi^2_{\rm min} = 15$. Even though the predicted radial velocity dispersion of this model does decrease with radius, this decline is of insufficient amplitude to reproduce the trend shown by the data. Note that this model, motivated by dark matter simulations, provides a poorer fit than the constant β model. Models where the velocity ellipsoid becomes more tangentially anisotropic with radius, $\beta-\mathrm{tg_{toy}}$ and $\beta-\mathrm{tg_{SN}}$, follow very well the data and have $\chi^2_{\rm min} = 6$ and 7, respectively. We find that, for model $\beta-\mathrm{tg_{toy}}$, the best-fitting virial mass is $M_{\rm v} = 8.8\ (\pm0.7, \pm1.2) \times 10^{11}\ \mathrm{M}_\odot$ (at the 1σ, 2σ level) and, for $\beta-\mathrm{tg_{SN}}$, $M_{\rm v} = 1.5\ (\pm0.1, \pm0.2) \times 10^{12}\ \mathrm{M}_\odot$ (at the 1σ, 2σ level). For the $\beta-\mathrm{tg_{toy}}$ model, we find that mass enclosed in 120 kpc is $M(<120\,\mathrm{kpc}) = 5.9 \pm 0.5 \times 10^{11}\ \mathrm{M}_\odot$; for the $\beta-\mathrm{tg_{SN}}$ model, $M(<120\,\mathrm{kpc}) = 9.0 \pm 0.6 \times 10^{11}\ \mathrm{M}_\odot$. Table 2 summarizes the best-fitting parameters for our favourite models.

This analysis highlights the mass–velocity anisotropy degeneracy, because it shows that, even for the same functional form of β, the best-fitting value of the virial mass can differ by a factor of 2. Note that the best-fitting values of the virial mass for the $\beta-\mathrm{tg_{toy}}$ model and the $\beta =$ constant are very comparable, but this is a reflection of the fact that the two anisotropy parameters are not too similar throughout a fair range of the distances probed by the sample.

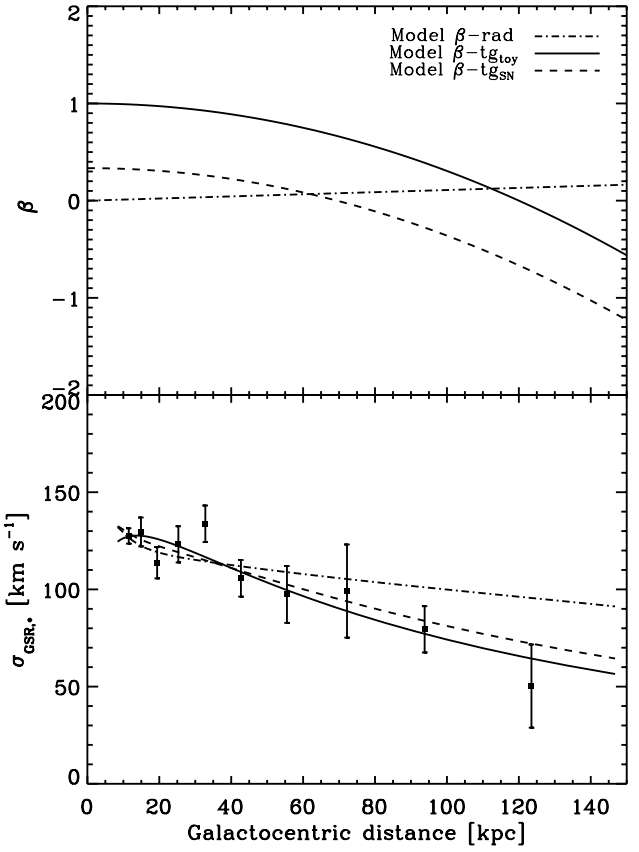

Figure 6. Top: the solid and dashed curves correspond to two toy models for a velocity ellipsoid that becomes more tangentially anisotropic with radius. The dashed-dotted line shows a model for an increasingly radially anisotropic ellipsoid from Diemand et al. (2004). Bottom: best-fitting models for an NFW halo of concentration $c = 18$ corresponding to the β profiles shown in the top panel.

Table 2. Values of the parameters for our favourite best-fitting models; the scalelength corresponds to a for the TF model and r_v for the NFW.

	$\chi^2_{\rm min}$	β	Mass $[10^{12}\,{\rm M}_\odot]$	Scalelength [kpc]
TF model	25	-0.5	$1.2^{+1.8}_{-0.5}$	105
NFW model	12	0.94	$0.8^{+1.2}_{-0.2}$	255 ($c = 18$)
NFW model ($\beta-{\rm tg}_{\rm SN}$)	7	$\beta'(r) < 0$	1.5±0.1	312 ($c = 18$)

However, because the value of β in the Solar neighbourhood is in the range 0.5 ± 0.1 (Chiba & Yoshii 1998), this would tend to suggest that, given that the ellipsoid needs to be tangentially anisotropic at large radii to give a good fit to the data, a higher value of the total mass is more likely.

If we apply the same kind of analysis to the pseudo-isothermal sphere mass model, it is clear that β has to decrease more strongly with radius than the above $\beta-$tg model used in combination with the NFW profile in order to give a reasonable fit to the data. This is in line with the results of Sommer-Larsen et al. (1997). By assuming a logarithmic potential for the dark matter halo, they found a velocity ellipsoid radially anisotropic at the Solar circle ($\beta \sim 0.5$) and tangentially anisotropic for $r \gtrsim 20$ kpc. At $r \sim 50$ kpc, the expected value of $\beta \sim -1$. The Sommer-Larsen et al. (1997) model is consistent with our findings out to ∼50 kpc; however, if we extrapolate the predicted trend for β to larger Galactocentric distances, we notice that β does not decrease sufficiently rapidly to explain the decline observed in our data (see also Appendix B).

From the above analysis, it is evident that assumptions on β for a particular mass model can strongly influence the performance of the mass model. However, not all functional forms of β for a given mass model produce a good fit to the data. More accurate proper motion measurements for a larger number of halo tracers and covering a larger range in Galactocentric distances will enable us to understand which trend in radius β is following and, therefore, to establish more uniquely which mass model is preferred by the data.

In addition to varying the velocity anisotropy parameter β as a function of radius, it is also possible to consider the effect of changing the slope γ of the stellar density profile of the Galactic halo. In this case, however, the data is much more restrictive in the choice of possible models, because it is well known that $\gamma \sim 3$–3.5 out to ~ 50 kpc (Yanny et al. 2000). Equation (2) shows that possible variations of the stellar halo power law γ with radius can 'conspire' with variations of β to reproduce the same radial velocity dispersion profile. We examine this issue further in Appendix B.

3 DISCUSSION AND CONCLUSIONS

We have derived the radial velocity dispersion profile of the stellar halo of the Milky Way using a sample of 240 halo objects with accurate distance and radial velocity measurements. The new data from the Spaghetti survey led to a significant increase in the number of known objects for Galactocentric radii beyond 50 kpc, which allowed a more reliable determination of the dispersion profile out to very large distances. Our most distant probes are located at ∼120 kpc, which in comparison to previous works (e.g. Sommer-Larsen et al. 1997) corresponds to an increase of 70 kpc in probing the outer halo. The Galactocentric radial velocity dispersion measured is approximately constant ($\sigma_{\rm GSR,*} \sim 120\,{\rm km\,s^{-1}}$) out to 30 kpc (consistent with Ratnatunga & Freeman 1989) and then it shows a continuous decline out to the last measured point (50 ± 22 km s^{-1} at 120 kpc). This fall-off has important implications for the density profile of the dark matter halo of the Milky Way. In particular, in the hypothesis of a constant velocity anisotropy, an isothermal sphere can be immediately ruled out as model for the Galactic dark halo as this predicts a nearly constant radial velocity dispersion curve.

We have also considered two other possible models for the dark halo: a TF and an NFW profile. We have compared the radial velocity dispersion observed with that predicted in these models for a tracer population (stellar halo) embedded in a potential provided by the dark halo. By means of a χ^2 test, we were able to derive the characteristic parameters and velocity anisotropy of these models that are most consistent with the observed data.

In the case of a TF profile, the favourite model for the Milky Way dark matter halo has a mass $M = 1.2^{+1.8}_{-0.5} \times 10^{12}\,{\rm M}_\odot$, with a corresponding velocity anisotropy $\beta = -0.50 \pm 0.4$. The data are also compatible with an NFW dark halo of $M_{\rm v} = 0.8^{+1.2}_{-0.2} \times 10^{12}\,{\rm M}_\odot$ and $-0.3 \lesssim \beta \lesssim 1$ for a concentration $c = 18$. The comparison of the fits produced by the constant anisotropy TF and NFW models shows that the latter reproduces better the trends in the data as a whole, from small to large radii. However, at very large radii it tends to overpredict the velocity dispersion. In this regime, the TF model, having a steeper density profile, provides a much better fit.

Our determination of the dark halo mass of the Milky Way is consistent with previous works: the preferred TF model of W&E99 gives a mass $M = 1.9 \times 10^{12}\,{\rm M}_\odot$, with a 1σ range of $0.2 < M[10^{12}\,{\rm M}_\odot] < 5.5$ and $-0.4 < \beta < 0.7$; the favourite model from Klypin et al. (2002) gives $M = 1.0 \times 10^{12}\,{\rm M}_\odot$ with $c = 12$. However, the radial velocity dispersion predicted by these two models is larger than the observed one. The discrepancy between the observed low values of the radial velocity dispersion at large radii and that predicted for heavy dark haloes raises the question of whether the velocity dispersion in the two most distant bins may be affected by systematics, such as the presence of streams, which could lower their values.

The two bins in question are centred at ∼90 and ∼120 kpc and contain six and three objects, respectively: four satellite galaxies and five globular clusters. The minimum angular separation of any two objects in these bins is 40°, for the satellites and 49° for the GCs. When considering the sample with nine objects, only two of these objects appear to be close on the sky: one globular cluster and one satellite galaxy that are located at $(l, b) \sim (241°, 42°)$. Although these are at similar distances of 96 and 89 kpc, respectively, their line-of-sight radial velocities differ by more than 140 km s^{-1}, thus making any physical association extremely unlikely.

We have also investigated the effect of a velocity anisotropy that varies with radius on the velocity dispersion $\sigma_{\rm GSR,*}$ in the case of an NFW halo of concentration $c = 18$. We find that the velocity anisotropy, which is radial at the Solar neighbourhood, needs to become more tangentially anisotropic with radius in order to fit the observed rapid decline in $\sigma_{\rm GSR,*}$. In the case of an isothermal dark matter halo, the β profile needs to decline even more steeply than in the NFW case in order to fit the data.

We conclude that the behaviour of the observed velocity dispersion can be explained either by a dark matter halo following a steep density profile at large radii and constant velocity anisotropy, or by a halo with a less steep profile whose velocity ellipsoid becomes tangentially anisotropic at large radii. In order to distinguish between an NFW profile and a TF model, proper motions are fundamental because they enable the direct determination of the velocity anisotropy profile. Proper motions of GCs and satellites are becoming available

(Dinescu, Girard & van Altena 1999; Piatek et al. 2003; Dinescu et al. 2004) albeit with large errors because of the very distant location of these objects. We may have to wait until *Gaia* is launched to determine the density profile of the Galactic dark matter halo.

ACKNOWLEDGMENTS

Giuseppina Battaglia gratefully acknowledges Eline Tolstoy. We thank Simon White and the anonymous referee for useful suggestions. This research has been partially supported by the Netherlands Organization for Scientific Research (NWO) and the Netherlands Research School for Astronomy (NOVA). HM, EWO and MM acknowledge support from the NSF on grants AST 96-19490, 00-98435, 96-19524, 00-98518, 95-28367, 96-19632 and 00-98661. We used the web catalogue http://physwww.mcmaster.ca/~harris/mwgc.dat for the Milky Way globular cluster data.

REFERENCES

Beers T. C., Chiba, M., Yoshii Y., Platais I., Hanson R. B., Fuchs B., Rossi S., 2000, AJ, 119, 2866
Bellazzini M., 2004, MNRAS, 347, 119
Binney J., Tremaine S., 1987, Galactic Dynamics. Princeton Univ. Press, Princeton, NJ
Bissantz N., Debattista V. P., Gerhard O., 2004, ApJ, 601, L155
Bullock J. S., Kolatt T. S., Sigad Y., Somerville R. S., Kravtsov A. V., Klypin A. A., Primack J. R., Dekel A., 2001, MNRAS, 321, 559
Carretta E., Gratton R. G., Clementini G., Pecci F. F., 2000, ApJ, 533, 215
Chiba M., Yoshii Y., 1998, AJ, 115, 168
Clewley L., Warren S. J., Hewett P. C., Norris J. E., Peterson R. C., Evans N. W., 2002, MNRAS, 337, 87
Clewley L., Warren S. J., Hewett P. C., Norris J. E., Peterson R. C., Evans N. W., 2004, MNRAS, 352, 285
de Blok W. F. G., McGaugh S., Rubin V., 2001, AJ, 122, 2396
Dehnen W., Binney J., 1998, MNRAS, 294, 429
Diemand J., Moore B., Stadel J., 2004, MNRAS, 352, 535
Dinescu D. I., Girard T. M., van Altena W. F., 1999, AJ, 117, 1792
Dinescu D. I., Keeney B. A., Majewski S. R., Girard T. M., 2004, AJ, 128, 687
Evans N. W., Binney J., 2001, MNRAS, 327, L27
Fich M., Tremaine S., 1991, ARA&A, 29, 409
Gao L., De Lucia G., White S. D. M., Jenkins A., 2004, MNRAS, 352, 1
Ghigna S., Moore B., Governato F., Lake G., Quinn T., Stadel J., 1998, MNRAS, 300, 146
Harris W. E., 1996, AJ, 112, 1487
Honma M., Sofue Y., 1997, PASJ, 49, 453
Jaffe W., 1983, MNRAS, 202, 995
Klypin A., Zhao H., Somerville R. S., 2002, ApJ, 573, 597
Kochanek C. S., 1996, ApJ, 457, 228
Kroupa P., Bastian U., 1997, New Astron., 2, 77
Mateo M., 1998, ARA&A, 36, 435
Morrison H., Mateo M., Olszewski E. W., Harding P., Dohm-Palmer R. C., Freeman K. C., Norris J. E., Morita M., 2000, AJ, 119, 2254
Morrison H. et al., 2003, AJ, 125, 2502
Navarro J. F., Frenk C. S., White S. D. M., 1997, ApJ, 490, 493
Perryman M. A. C. et al., 2001, A&A, 369, 339
Piatek S., Pryor C., Olszewski E. W., Harris H. C., Mateo M., Minniti D., Tinney C. G., 2003, AJ, 126, 2346
Ratnatunga K., Freeman K. C., 1989, ApJ, 339, 126
Rohlfs K., Kreitschmann J., 1988, A&A, 201, 51
Romanowsky A. J., Douglas N. G., Arnaboldi M., Kuijken K., Merrifield M. R., Napolitano N. R., Capaccioli M., Freeman K. C., 2003, Sci, 301, 1696
Sakamoto T., Chiba M., Beers T. C., 2003, A&A, 397, 899 (SCB03)
Schweitzer A. E., Cudworth K. M., Majewski S. R., Suntzeff N. B., 1995, AJ, 110, 2747
Schweitzer A. E., Cudworth K. M., Majewski S. R., 1997, PASP, 127, 103
Sirko E. et al., 2004a, AJ, 127, 914
Sirko E. et al., 2004b, AJ, 127, 899
Sommer-Larsen J., Beers T. C., Flynn C., Wilhelm R., Christensen P. R., 1997, ApJ, 481, 775
Taylor J. E., Babul A., Silk J., 2004, in Prada F., Martinez-Delgado D., Mahoney T. J., eds, ASP Conf. Ser. Vol. 327, Satellites and Tidal Streams. Astron. Soc. Pac., San Francisco, p. 205
Wechsler R. H., Bullock J. S., Primack J. R., Kravtsov A. V., Avishai D. A., 2002, ApJ, 568, 52
White S. D. M., 1983, ApJ, 274, 53
Wilhelm R., Beers T. C., Sommer-Larsen J., Pier J. R., Layden A. C., Flynn C., Rossi S., Christensen P. R., 1999, AJ, 117, 2329
Wilkinson M., Evans N. W., 1999, MNRAS, 310, 645 (W&E99)
Yanny et al., 2000, ApJ, 540, 825
Zaritsky D., Olszewski E. W., Schommer R. A., Peterson R. C., Aaronson M., 1989, ApJ, 345, 759

APPENDIX A

The Galactocentric radial velocity $v_{\rm GSR}$ (i.e. the line-of-sight heliocentric velocity $V_{\rm los}$ corrected for the solar motion and LSR motion) is related to the true Galactocentric radial, $V_{\rm r}$, and tangential, $V_{\rm t}$, velocity by

$$V_{\rm GSR} = V_{\rm r}\,\hat{\boldsymbol{\epsilon}}_{\rm r}\cdot\hat{\boldsymbol{\epsilon}}_{\rm R} + V_{\rm t}\,\hat{\boldsymbol{\epsilon}}_{\rm t}\cdot\hat{\boldsymbol{\epsilon}}_{\rm R} \tag{A1}$$

where $\hat{\boldsymbol{\epsilon}}_{\rm r}$ is the unit vector in the radial direction towards the object as seen from the Galactic Centre, $\hat{\boldsymbol{\epsilon}}_{\rm t}$ is the unit vector in tangential direction in the same reference frame and $\hat{\boldsymbol{\epsilon}}_{\rm R}$ is the unit vector in the radial direction from the Sun to the object. The two scalar products depend on the heliocentric and galactocentric distances (d and r) and position on the sky of the object (ϕ, θ). For a given distribution function $f(\bar{r}, \bar{V})$, the velocity dispersion profile (seen from the Sun) is given by $\sqrt{\langle V^2_{\rm GSR}\rangle}$ and can be found by squaring equation (A1) and integrating over all the velocities and averaging over the solid angle:

$$\left\langle V^2_{\rm GSR}\right\rangle\Big|_{\Omega-{\rm av}} = \frac{1}{\int {\rm d}^2\Omega}\left[\int {\rm d}^2\Omega\, k(r,\theta,\phi)\int {\rm d}^3V\, V_{\rm r}^2\, f(\bar{r},\bar{V}) + \int {\rm d}^2\Omega\, h(r,\theta,\phi)\int {\rm d}^3V\, V_{\rm t}^2\, f(\bar{r},\bar{V})\right],$$

or

$$\left\langle V^2_{\rm GSR}\right\rangle\Big|_{\Omega-{\rm av}} = \frac{1}{4\pi}\left[\int {\rm d}^2\Omega\, k(r,\theta,\phi)\left\langle V_{\rm r}^2\right\rangle + \int {\rm d}^2\Omega\, h(r,\theta,\phi)\left\langle V_{\rm t}^2\right\rangle\right], \tag{A2}$$

where we have defined

$$\hat{\boldsymbol{\epsilon}}_{\rm R} = \frac{\bar{r}-\bar{\rm R}_\odot}{d},$$

$$k(r,\theta,\phi) = (\hat{\boldsymbol{\epsilon}}_{\rm r}\cdot\hat{\boldsymbol{\epsilon}}_{\rm R})^2 = \left(\frac{r+{\rm R}_\odot\,\cos\phi\,\sin\theta}{d}\right)^2$$

and

$$h(r,\theta,\phi) = (\hat{\boldsymbol{\epsilon}}_{\rm t}\cdot\hat{\boldsymbol{\epsilon}}_{\rm R})^2 = \frac{{\rm R}_\odot{}^2}{d^2}\,(\cos^2\theta\cos^2\phi+\sin^2\phi).$$

Equation (A2) can thus be expressed as

$$\left\langle V^2_{\rm GSR}\right\rangle\Big|_{\Omega-{\rm av}} = \left\langle V_{\rm r}^2\right\rangle K(r) + \left\langle V_{\rm t}^2\right\rangle H(r).$$

If we assume that $\langle V_\theta^2 \rangle = \langle V_\phi^2 \rangle$ and from the definition of the velocity anisotropy β, we find $\langle V_\mathrm{t}^2 \rangle = 2\,\langle V_\mathrm{r}^2 \rangle\,(1-\beta)$, then it follows that

$$\left\langle V_\mathrm{GSR}^2 \right\rangle\big|_{\Omega-\mathrm{av}} = \left\langle V_\mathrm{r}^2 \right\rangle [K(r) + 2(1-\beta)H(r)]. \quad \text{(A3)}$$

By assuming $\langle V_r \rangle = 0$ and $\langle V_\mathrm{t} \rangle = 0$, it follows that $\langle V_\mathrm{GSR} \rangle = 0$; by performing the above integrals for $r > \mathrm{R}_\odot$, we find that the Galactocentric radial velocity dispersion is related to the true radial velocity dispersion by

$$\sigma_\mathrm{GSR}(r) = \sigma_r(r)\,\sqrt{1 + 2\,(1-\beta)H(r)}, \quad \text{(A4)}$$

where

$$H(r) = \frac{r^2 + \mathrm{R}_\odot^2}{4r^2} - \frac{\left(r^2 - \mathrm{R}_\odot^2\right)^2}{8r^3\mathrm{R}_\odot} \ln\frac{r + \mathrm{R}_\odot}{r - \mathrm{R}_\odot}. \quad \text{(A5)}$$

APPENDIX B

Equation (2) shows that the radial velocity dispersion profile depends on the circular velocity given by the dominant mass component (i.e. the dark matter halo), the velocity anisotropy parameter β and the power γ of the density profile of the tracer population. For constant β and γ, we can rewrite equation (2) as

$$\sigma^2{}_{r,*}(r) = \frac{1}{r^{2\beta-\gamma}} \int_\mathrm{r}^\infty V_\mathrm{c}^2(r')\, r'^{\,2\beta-\gamma-1}\, \mathrm{d}r'. \quad \text{(B1)}$$

In our work, we assumed $\gamma = 3.5$ at all Galactocentric distances, but the above equation shows also that, for a fixed mass distribution (i.e. fixed circular velocity), models with the same value for $2\beta - \gamma$ give rise to the same radial velocity dispersion profile. In this section, we explore how β or γ have to vary together in order to reproduce the observed Galactocentric radial velocity dispersion.In this analysis, we restrict ourselves to Galactocentric distances larger than 40 kpc, where: the value of γ starts to become more uncertain; the observed Galactocentric radial velocity dispersion declines; and the correction factor between the Galactocentric and the true radial velocity dispersions is negligible.

At these distances, the Galactocentric radial velocity dispersion profile is well represented by a straight line, $\sigma_{\mathrm{GSR,fit}} = a\,r + b$, with $a = -0.6$ and $b = 132$ (Fig. B1, first panel). We assume that the circular velocity for the dark matter halo is constant and we fix it to $V_\mathrm{c}(r) = V_\mathrm{c} = 220\,\mathrm{km\,s^{-1}}$. By solving equation (2), we obtain

$$\sigma^2_{r,*} = \frac{V_\mathrm{c}^2}{\gamma - 2\beta}. \quad \text{(B2)}$$

For all the values of β and γ that satisfy this relation (at every r), the predicted radial velocity dispersion curve will be the same. By imposing $\sigma^2_{r,*} = \sigma^2_{\mathrm{GSR,fit}}$ in equation (B1), it follows

$$\gamma - 2\beta = \frac{V_\mathrm{c}{}^2}{\sigma^2_{\mathrm{GSR,fit}}}. \quad \text{(B3)}$$

Fig. B1 (second panel) shows the above relation for the assumed model. The third panel in Fig. B1 shows how β has to vary with the Galactocentric distance for this model if we fix $\gamma = 3.5$, whilst the panel on the right shows how γ has to change if we use the $\beta-\mathrm{tg}_\mathrm{SN}$ model for β. Clearly, for this model, the values the γ should assume in order to reproduce the data are unrealistic.The same kind of relation between β and γ can be derived for different circular velocities in the regime where they can be approximated by power laws.

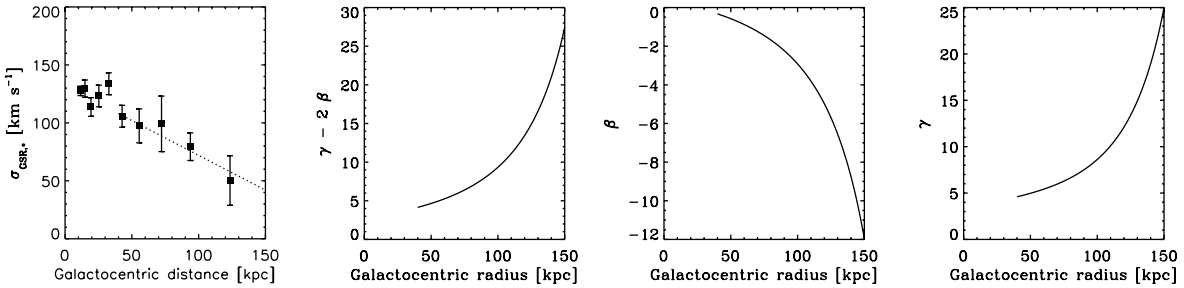

Figure B1. First panel: observed Galactocentric radial velocity dispersion (squares with error bars); the dotted line is a straight line fit for $r > 40$ kpc. Second panel: relation β and γ should satisfy to result in the same $\sigma_{\mathrm{GSR},*}$. Third panel: variation of β with radius fixing $\gamma = 3.5$. Fourth panel: variation of γ with radius fixing β to the $\beta-\mathrm{tg}_\mathrm{SN}$ model.

This paper has been typeset from a TEX/LATEX file prepared by the author.